Tailoring the surface termination of $BiVO_4$ photoanodes using ammonium metavanadate enhances the solar water oxidation performance

Qingjie Wang[a,b], Zeyuan Wang[a], Nan Liao[a], Salvador Montilla[b], Maxime Contreras[b], Néstor Guijarro[b,*], Jingshan Luo[a,c,d,*]

[a]*Institute of Photoelectronic Thin Film Devices and Technology, State Key Laboratory of Photovoltaic Materials and Cells, Key Laboratory of Photoelectronic Thin Film Devices and Technology of Tianjin, Ministry of Education Engineering Research Center of Thin Film Photoelectronic Technology, Nankai University, Tianjin 300350, China*
[b]*Institute of Electrochemistry, Universidad de Alicante, Apartat 99, E-03080 Alacant, Spain*
[c]*Frontiers Science Center for New Organic Matter, Nankai University, Tianjin 300071, China*
[d]*Haihe Laboratory of Sustainable Chemical Transformations, Tianjin 300192, China*
**Email: jingshan.luo@nankai.edu.cn, nestor.guijarro@ua.es*

Abstract:
Altering the surface stoichiometry of semiconductor electrodes is known to affect the photoelectrochemical (PEC) response. To date, several reports have hinted at the influence of the surface Bi:V ratio on the solar water oxidation performance of $BiVO_4$ photoanodes, but only a handful of strategies have been reported to afford to fine-tune such surface stoichiometry while a comprehensive understanding of an atomic level of the role of the surface termination remains elusive. Herein, we report a new methodology that modulates the surface Bi:V ratio and, in turn, maximizes the PEC performance towards the oxygen evolution reaction (OER). We found that annealing in the presence of ammonium metavanadate drastically reduces the surface recombination while improving the charge separation. Detailed characterization revealed that this treatment filled the native surface vanadium vacancies, which are found to act as recombination centers, while inducing a significant increase in the density of oxygen vacancies, which reinforced the built-in electric field that drives the charge separation. Interestingly, coating with $NiFeO_x$ improves, especially, the charge separation in surface V-rich $BiVO_4$. Results suggest that the V-rich surface termination altered the surface energetics of $BiVO_4$ leading to an improved band alignment across the interface. Overall, these results provide a new platform to modulate the surface stoichiometry of $BiVO_4$ thin films while shedding new light on the mechanisms whereby the surface termination governs the PEC response.

Keywords: Photoelectrochemical water oxidation, $BiVO_4$ photoanode, surface stoichiometry, ammonium metavanadate, bulk composition.

Introduction

Photoelectrochemical (PEC) water splitting stands out as one of the most attractive approaches for sourcing hydrogen sustainably and cost-effectively.[1, 2] Tandem cells, including both a semiconductor photocathode and a photoanode to perform separate water reduction and oxidation, are the prevalent architecture. $BiVO_4$ photoanodes have been drawing increasing attention owing to their relatively narrow band gap and suitable band energy level positions; the latter affording one of the lowest photocurrent onset potentials (*i.e,* turn-on voltage, V_{on}) amongst metal oxides (ca. 0.2 V vs RHE).[3,4] However, the severe surface and bulk recombination, together with the slow water oxidation kinetics[5,6] and the photocorrosion of the material, have thus far limited the performance and the operational lifespan of such photoanodes.

To date, several strategies have been investigated to address the intrinsic issues of $BiVO_4$ photoanodes.[7-9] On the one hand, the deposition of co-catalysts, such as CoPi, $NiFeO_x$ or VO_x, has been proven to effectively mitigate the surface recombination and accelerate the OER while preventing photocorrosion.[5,6,10-12] On the other hand, altering the bulk composition of $BiVO_4$, for instance, controlling the oxygen vacancy content or intentionally doping with Mo or W, amongst others, has been shown to improve the conductivity and promote the photogenerated charge carriers' separation.[13-15] However, the role that the semiconductor's termination plays on the PEC response and whether it could

be fine-tuned to patch some of the surface-derived issues detected on $BiVO_4$ photoanodes remains barely unexplored.

Recently, Choi and co-workers brought out this topic by demonstrating that controlling the surface Bi:V ratio drastically affects the PEC performance.[16,17] Using epitaxially-grown $BiVO_4$ thin films and controlling the etching time to preferentially strip vanadium atoms, the authors managed to modulate the surface Bi:V ratio. It was found that Bi-rich samples afford higher photocurrent values and earlier photocurrent onset potential owing to the more suitable surface energetics. Likewise, follow-up work of these authors confirmed that the surface termination controlled the charge transfer between the $BiVO_4$ semiconductor, and the co-catalyst deposited on top.[17] Alternatively, Lu et al. demonstrated that inducing Bi vacancies, and therefore, a V-rich surface, improved the bulk carrier transport and the interfacial charge transfer,[18] leading to an amelioration of the PEC response. Alternatively, Phu et al. showed that the presence of V vacancies creates a new sub-band gap near the Fermi level, increasing the recombination rate of electron-hole pairs.[19] Therefore, although a considerable body of work has pointed out that the surface Bi:V ratio dictates the performance,[20] there are, so far, just a handful of strategies to engineer the atomic termination in a controlled manner, while the impact of the surface composition on the fundamental parameters that govern the PEC response remains to be elucidated.

Here, in this study, we report for the first time on the use of an ammonium metavanadate (NH_4VO_3) post-treatment to adjust the surface Bi:V ratio on $BiVO_4$ photoanodes. We found that increasing the surface vanadium content causes not only the saturation photocurrent to increase but also, the V_{on} to shift about 200 mV towards more negative potentials. Detail characterization revealed that V-rich surface led to a drastic enhancement in the interfacial charge transfer resulting, primarily, from the mitigation of the surface recombination and the upward shift of the energy bands. Subsequent coating with the state-of-the-art $NiFeO_x$ catalyst further improved the performance, especially, of the V-rich sample, thus evidencing the impact of the atomic termination on the behavior of the catalytic overlayer.

Results and discussion

Nanostructured $BiVO_4$ thin films were fabricated following the protocol reported by Kim et al. with minor changes.[21] Subsequent modification of the native surface Bi:V ratio was carried out by annealing pristine $BiVO_4$ at an optimized temperature of 350 ºC (*vide infra*) in the presence of NH_4VO_3 under a constant flow of nitrogen gas (**Scheme 1**). Note that NH_4VO_3 has been previously employed as V precursors to synthesize CVD-grown V-doped MoS_2.[22] Controlled experiments performed using BiOI, instead of $BiVO_4$, as substrate confirmed the incorporation of vanadium upon NH_4VO_3 treatment (Figure S1).

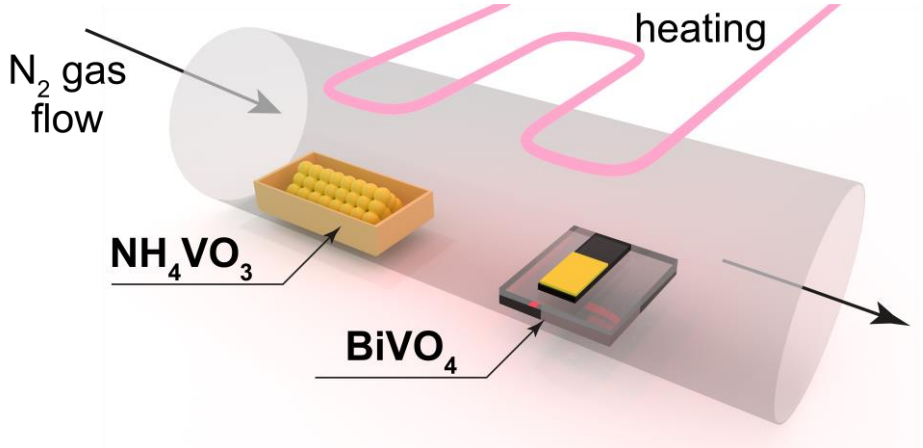

Scheme 1. Illustration of the NH_4VO_3 treatment indicating the relative position of the NH_4VO_3 and the $BiVO_4$ thin film electrode.

Figure 1a shows the X-ray diffraction (XRD) patterns recorded for pristine $BiVO_4$, and NH_4VO_3-treated $BiVO_4$ as a function of the annealing time, denoted as V-$BiVO_4$-X, where X indicates the time (minutes) of the treatment. As observed, all diffraction peaks can be well indexed to the reference patterns of the monoclinic structure of $BiVO_4$ (JCPDS PDF #14-0688) and of the SnO_2 present in the

conductive substrate (JCPDS PDF #46-1088). Note that no noticeable changes were observed in the diffractograms upon the NH_4VO_3 treatment. Likewise, **Figure S2** displays the UV-Vis absorption spectra for pristine and NH_4VO_3-treated samples demonstrating that the optical characteristics remained virtually unchanged. In all cases, an onset of absorption at ca. 500 nm corresponding to a band gap of 2.50 eV was estimated. To assess the impact of the NH_4VO_3 treatment on the atomic termination, the surface composition was examined by X-ray photoelectron spectroscopy (XPS). **Figure 1b** shows the surface Bi:V ratio as a function of the annealing time. Note that in all cases the surface is Bi-rich rather than near to stoichiometric, and the NH_4VO_3 treatment gradually reduces the Bi:V ratio with increasing annealing time. Finding a Bi-rich surface is not unexpected and, indeed, the Bi:V ratio detected in the pristine sample matches well with that reported by other authors that followed the same synthetic approach.[23] This unbalanced surface stoichiometry has been previously ascribed to a commonplace phase segregation occurring in bismuth-containing oxides that results in an excess Bi and oxygen on the surface.[24] Interestingly, by adjusting the time of the NH_4VO_3 treatment it is possible to fine-tune the surface Bi:V ratio from 2.3 to 1.3. The mechanism whereby the V atoms are incorporated in the structure is not yet clear. We hypothesize that the incoming vanadium fills existing V vacancies or, as recently proposed, the lower energy formation of Bi vacancies affords the incorporation of V in the lattice by cation exchange.[25]

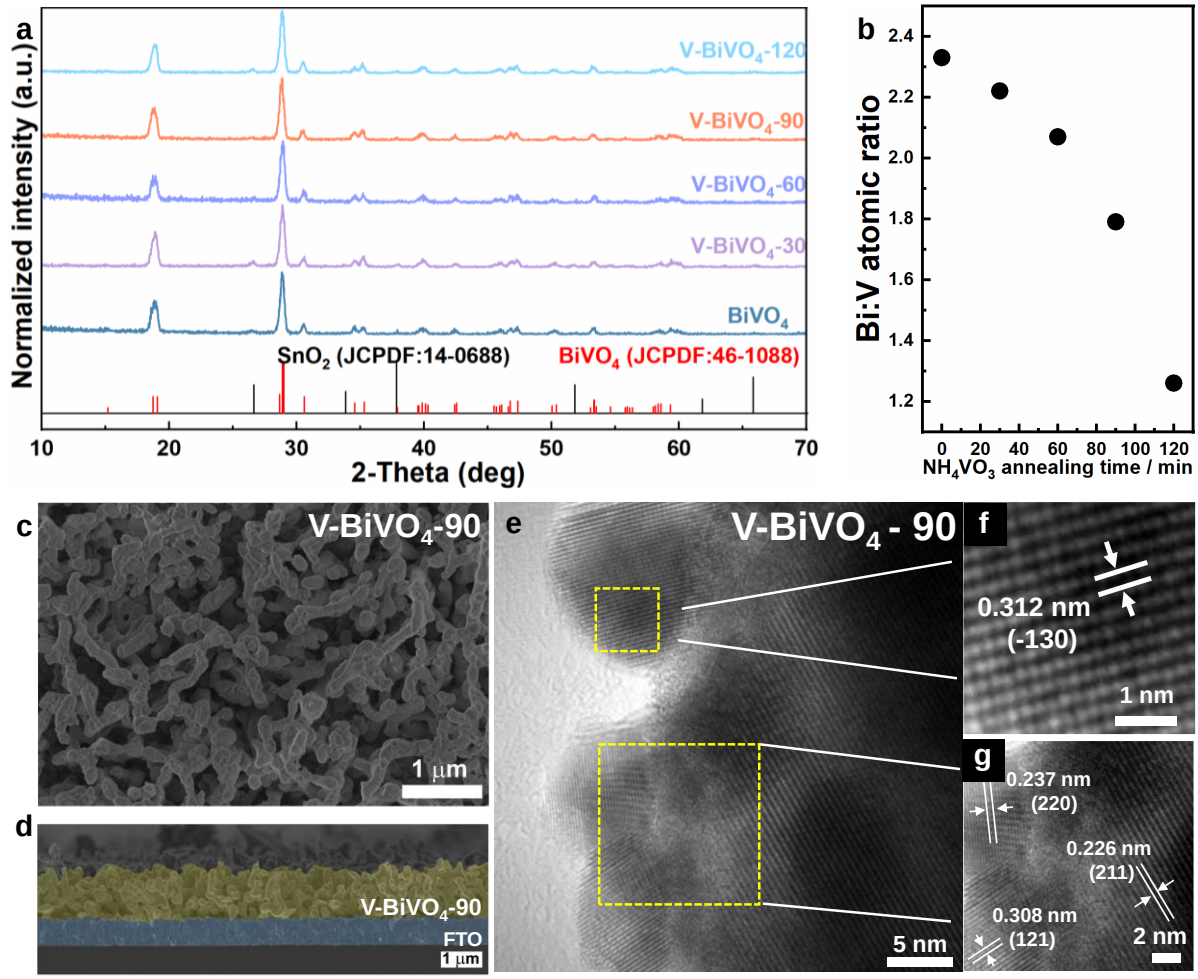

Figure 1. (a) X-ray diffraction (XRD) patterns for pristine and NH_4VO_3-treated samples for different annealing times. (**b)** Surface Bi:V atomic ratio as a function of the NH_4VO_3 treatment time. (**c)** Top-view scanning electron microscopy (SEM) image of V-$BiVO_4$-90 sample and (**d)** the corresponding cross-section image. (**e, f, g)** High resolution transmission electron microscopy (HRTEM) images of V-$BiVO_4$ photoanode.

Next, the morphology of the thin film electrodes was examined by using scanning electron microscopy (SEM). The top-view and cross-sectional SEM images obtained for a representative NH_4VO_3-treated

sample (V-$BiVO_4$-90) revealed the characteristic worm-like nanoporous structure, typically reported for this synthetic route.[5,21] Here, the nanorods displayed an average diameter of approx. 200-300 nm whereas the film is about 1.0 μm thick (**Figure 1c,d**). Energy-dispersive X-ray (EDX) spectroscopy measurements revealed an average bulk Bi:V ratio of 1.1:1.0, i.e., close to stoichiometric. We note that no apparent differences were detected when compared to the pristine sample (Figure S3). Likewise, to gain more insights on the nanoscopic structure and the distribution of the elemental components, transmission electron microscopy (TEM) images were collected. The high-resolution TEM (HR-TEM) image of V-$BiVO_4$-90 evidenced the polycrystalline nature of the material (**Figure 1e**). Detailed analysis of the lattice fringes reveals interplanar spacings of 0.312 ± 0.01 nm and 0.226 ± 0.01 nm that correspond, respectively, to the (-130) and (211) planes (**Figure 1f, g**), of the monoclinic $BiVO_4$ phase. Careful examination of V-$BiVO_4$-90 nanoparticles employing EDX spectroscopy measurements reveals a stoichiometric composition (Bi:V:O) and an even distribution of the elements ruling out, in principle, the formation of a distinct VO_x layer upon the treatment (Table S1 and S2). Similarly, the EDX line scanning spectrum did not provide evidence that supports the formation of a distinct VO_x layer at the surface (Figure S4). We note that, unlike in these samples, previous reports dealing with surface V-rich $BiVO_4$ are coated by a noticeable few-nm-thick VO_x layer.[25, 26]

To investigate how the NH_4VO_3 treatment affects the chemical state of the surface elements, the high-resolution XPS spectra of Bi 4f, V 2p and O 1s were collected for pristine and NH_4VO_3-modified $BiVO_4$ films (**Figure 2**). Firstly, for the Bi 4f, core-level XPS spectra portray two symmetrical bands corresponding to the Bi $4f_{5/2}$ and Bi $4f_{7/2}$ doublet,[27] exhibiting in all cases a spin-orbit splitting value of 5.3 eV. In the case of the pristine sample, the Bi $4f_{5/2}$ and $4f_{7/2}$ components are located at 164.3 and 159.0 eV, respectively These results coincide with previous reports on $BiVO_4$ and confirm the presence of Bi^{3+}. Note that the deconvolution did not yield any additional bands that could be linked to the presence of Bi_2O_3.[28,29] Interestingly, prolonged NH_4VO_3 treatments caused a shift towards lower binding energies on these bands, suggesting that the electron density surrounding Bi centers is increasing. Secondly, the V 2p spectra show the two characteristic bands assigned to the V $2p_{1/2}$ and $2p_{3/2}$ components exhibiting a 7.6 eV spin-orbit splitting value. For the pristine sample, V $2p_{1/2}$ and $2p_{3/2}$ are centered at about 524.2 and 516.6 eV, respectively, which is typically ascribed to the presence of V^{5+} in $BiVO_4$.[27,29] It is worth noting that unlike in the case of Bi, no significant shift in the V 2p components was observed, except for long NH_4VO_3 treatments. Thirdly, the O 1s spectra display an asymmetric band that is commonly deconvolved into three contributions related to, namely, i) the chemically adsorbed oxygen species (or adsorbed water) (O_C), ii) oxygen vacancies (O_V), and iii) metal-oxygen bond from the lattice (O_L).[30-32] While the position of the bands appears to remain unaltered with the treatment, there is a noticeable increase in the O_V:O_L ratio with the annealing time, suggesting that the density of oxygen vacancies gradually increased in the topmost layer. A caveat, however, when considering this data is that the O_V signal that arises from low-coordinated oxygen could originate not only from oxygen vacancies, but from non-stoichiometric surface oxygen due to the poor crystallographic order or even from hydroxyl groups adsorbed on the surface that could appear in that same binding energy range.[33]

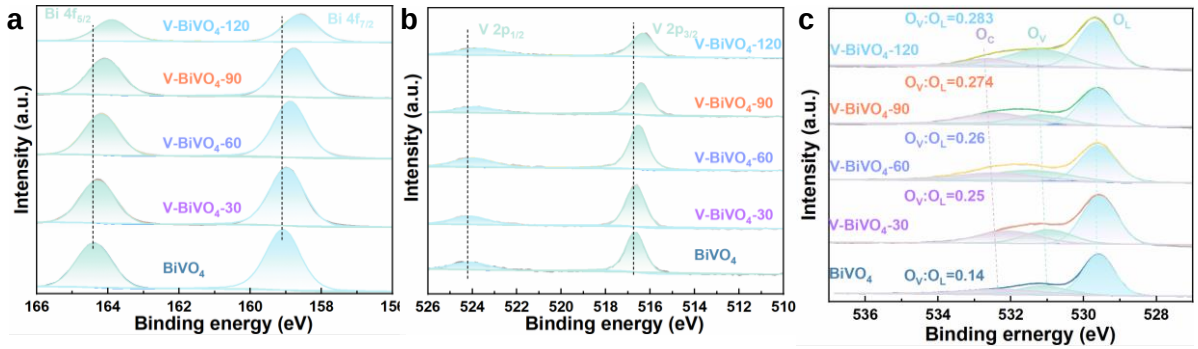

Figure 2. High-resolution X-ray photoelectron spectroscopy (XPS) spectra of (**a**)Bi 4f, (**b**) V 2p, (**c**) O 1s for $BiVO_4$, V-$BiVO_4$-30, V-$BiVO_4$-60, V-$BiVO_4$-90 and V-$BiVO_4$-120 photoanodes.

Based on the above XPS results we could draw the following conclusions. First, oxygen vacancies are generated at the surface, and likely, in the bulk of the material because of the NH_4VO_3 treatment. This is not unreasonable when considering that ammonia is released during the thermal decomposition of NH_4VO_3.[34] Note that annealing in the presence of ammonia has been demonstrated to induce the generation of oxygen vacancies in $BiVO_4$.[35] Second, the gradual shift of the Bi 4f bands could be ascribed to the preferential formation of oxygen vacancies in the vicinity of the Bi centers, that is, in the BiO_8 dodecahedra.[27] Third, the absence of a shift in the V 2p spectra, especially at shorter treatments, suggests that oxygen vacancies are mostly located in the BiO_8 dodecahedra, specially at the oxygen bridging two Bi sites instead of in the VO_4 tetrahedra. This could be accounted for by the fact that the V-O bond strength is much higher than that of the Bi-O, which would support the idea that the removal of oxygen atoms from the BiO_8 dodecahedra is more favorable than from the VO_4 tetrahedra.[36,37] Finally, the fact that neither an apparent shift towards higher binding energies nor an additional contribution in the V 2p components are detected, led us to assume that the incoming V incorporates preferentially in the available V vacancies rather than occupying Bi vacancies or exchanging surface Bi cations. Indeed, it is expected that the V 2p contributions will change drastically if the environment of the V center changes from tetrahedral (*i.e.*, VO_4) to dodecahedral (*i.e.*, the coordination of Bi centers).

Next, to explore the influence of the NH_4VO_3 treatment on the PEC water oxidation response, linear sweep voltammograms (LSVs) of both pristine and NH_4VO_3-treated samples were recorded under 1 sun illumination in standard KBi solution (pH=9.5). As shown in **Figure 3a**, the photocurrent values and the V_{on} increased with increasing treatment time from pristine $BiVO_4$ to V-$BiVO_4$-90, whereas longer annealing times appear to adversely affect the performance, as exemplified with V-$BiVO_4$-120. It is worth noting that the NH_4VO_3 treatment was performed at 350ºC based on the preliminary tests that revealed that carrying out the annealing at 300ºC or 400ºC was conducive to a lower PEC response (Figure S5). To further improve the PEC response, the state-of-the-art $NiFeO_x$ was photoelectrochemically deposited onto the surface. **Figure 3a** displays the LSVs obtained for bare and $NiFeO_x$-coated $BiVO_4$ and V-$BiVO_4$-90 (henceforth, V-$BiVO_4$) under chopped illumination. Comparison between $BiVO_4$ and V-$BiVO_4$, reveals that the NH_4VO_3 treatment affords to increase the photocurrent by ca. 40% (e.g., increasing from 1.43 mA/cm^2 to 1.98 mA/cm^2 at 1.0 V vs RHE), while shifting the V_{on} ca. 200 mV earlier. We note that the flat band potential (E_{FB}) determined by using the Mott-Schottky (MS) plot follows a similar behavior, shifting from 0.2 V ($BiVO_4$) to 0.15 V vs RHE (V-$BiVO_4$) (Figure S6, Table S3).

With the purpose of unravelling the operational parameters that are primarily impinged by the NH_4VO_3 treatment, and that are responsible for the improved PEC response, the charge separation (η_{sep}) and charge transfer efficiency (η_{tran}) were estimated (see experimental sections for details). Broadly speaking, η_{sep} represents the percentage of photogenerated holes that reach the interface, whereas η_{tran} indicates the percentage of surface holes that are transferred to the solution. As shown in **Figure 3b**, η_{sep} increases upon the NH_4VO_3-treatment, especially at small applied potentials, when it triggers a10% increase. The improved η_{sep} is commonly attributed to the strengthening of the built-in electric field at the space charge region. This, indeed, agrees well with fact that the carrier density, estimated via the MS plot (Figure S9), increased from 1.6×10^{18} cm^{-3} in pristine $BiVO_4$ to 2.1×10^{18} cm^{-3} in V-$BiVO_4$ which, likely, results from the higher density of oxygen vacancies detected upon the NH_4VO_3 treatment (Figure S9). In addition, and to corroborate this result, photovoltage (V_{ph}) measurements were undertaken, measured as the difference between the open circuit potential recorded in the dark and under illumination $\left(V_{ph} = E^{OCP}_{dark} - E^{OCP}_{light}\right)$ (**Figure 3c**, Figure S7). Bearing in mind that these tests were performed in the absence of a net current flow, they are not affected by the interfacial charge transfer across the interface and mostly reflect the bulk charge separation characteristics. As expected, V-$BiVO_4$ displays a V_{ph} that is about 30 mV larger than that of $BiVO_4$. This indicates that a larger population of photogenerated carriers can be accumulated within V-$BiVO_4$ under illumination, and thus, it supports the notion that charge separation is improved.

As shown in **Figure 3d**, the η_{tran} values drastically improved when moving from $BiVO_4$ to V-$BiVO_4$. Both the improved catalytic activity of the surface and the mitigation of the surface recombination have

been commonly invoked to explain this phenomenon. Dark LSVs for $BiVO_4$ and V-$BiVO_4$ were recorded to examine the electrocatalytic activity towards the OER (Figure S8). However, no change in the electroactivity was detected, ruling, therefore, out the influence of the surface catalysis on the improved η_{tran}. To monitor the influence of the NH_4VO_3 treatment on the surface recombination, the surface accumulated photogenerated holes were tracked by using fast-scan cyclic voltammograms (FS-CVs). **Figure 3e** shows representative FS-CVs recorded for $BiVO_4$ and V-$BiVO_4$ wherein two key features stand out, namely, the reversible cathodic and anodic band at around 1.0 V vs RHE, and the irreversible cathodic band centered at around 1.6 V vs RHE. The former reversible band is attributed to the fast redox process of V^{5+}/V^{4+}, which is believed to represent intrinsic surface states (i-SS) in the bulk that could indirectly mediate in the OER.[38] The latter, however, is considered to emerge from the accumulation of holes in surface traps that could not participate in the OER but rather act as recombination centers or surface states (r-SS).[39,40] As observed, the accumulated charge in the r-SS (Q_{r-SS}) plummets after the 1st cycle due to the irreversible emptying of the r-SS. Note that Q_{r-SS} drops in V-$BiVO_4$ compared to $BiVO_4$, suggesting that the density of r-SS decreases (**Figure 3f**). This could explain the mitigation of the deleterious surface recombination and the enhanced η_{tran} in V-$BiVO_4$. It is worth noting that literature reports, and control experiments where NH_4VO_3 was replaced by ammonium oxalate (Figure S8), to only introduce oxygen vacancies while maintaining the surface Bi:V unaltered, demonstrate (i) no change of the η_{tran}, but rather of the η_{sep},[27] (ii) no difference on the electrocatalytic response, and thus, no effect on the OER catalysis, and (iii) no significant drop in Q_{r-SS}. With this in mind, we hypothesize that the r-SS originate from the occurrence of surface V vacancies, and thus, it is the filling of such defective sites in V-$BiVO_4$ what triggers the drop in Q_{r-SS}. This is indeed consistent with recent computational studies wherein the presence of V vacancies was demonstrated to cause the formation of surface trap states near the valence band edge.[19] We note that in-depth analysis of electrochemical impedance spectroscopy (EIS) data further supports the improved charge separation and transfer on the basis of the drastic drop on the estimated bulk and interfacial resistance (Figure S9, Table S4)). Overall, it is worth highlighting that the change of the η_{tran} is larger than that recorded for the η_{sep}.This strengthens the notion that it is the fine-tuning of the Bi:V ratio and the passivation of the surface trap states, rather than the induced oxygen vacancies, what dictated that improved PEC response towards the OER.

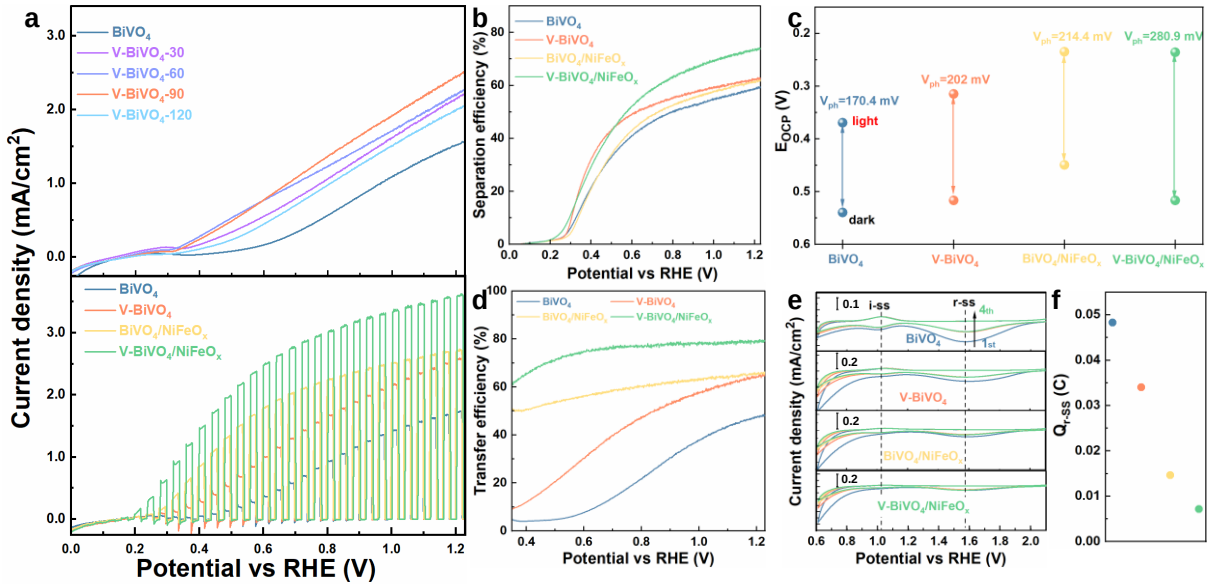

Figure 3. (a) LSVs recorded for pristine and NH_4VO_3-treated $BiVO_4$ films under continuous illumination (top) and for representative films prior and after coating with $NiFeO_x$ under chopped irradiation (bottom). **(b)** Charge separation efficiency (η_{sep}) and **(c)** stabilized open circuit potential (OCP) values in dark and under illumination. **(d)** Charge transfer efficiency (η_{trans}), **(e)** fast-scan cyclic voltammograms recorded at 0.3 V/s for 4 consecutive cycles, and **(f)** the estimated accumulated charge corresponding to the r-SS band.

Next, the state-of-the-art $NiFeO_x$ electrocatalyst was photoelectrodeposited onto both $BiVO_4$ and V-$BiVO_4$ with the aim of further improving the PEC response. Electron microscopy and spectroscopy measurements confirmed the deposition of a thin homogeneous layer of the $NiFeO_x$ (Figure S10). As shown in **Figure 3a**, both the V_{on} and the photocurrent values were drastically improved. Firstly, the V_{on} shifted to 0.25 V vs RHE of the $BiVO_4$/$NiFeO_x$ and up to 0.19 V vs RHE for the V-$BiVO_4$/ $NiFeO_x$, that is about 250 mV and 110 mV earlier, respectively. Secondly, the photocurrent increased up to 2.7 mA/cm^2 and 3.61 mA/cm^2 at 1.2 V vs RHE, for $BiVO_4$ and V-$BiVO_4$, respectively. These values, although below the record photocurrent reported for $BiVO_4$ photoanodes (Table S5), show a distinct improvement with respect the pristine films. Interestingly, the photocurrent change after the $NiFeO_x$ coating is larger for the V-$BiVO_4$ (1.3 mA/cm^2) than for the $BiVO_4$ (0.9 mA/cm^2 at 1.2 V vs RHE). This result, at a first glance, appears counterintuitive, since pristine V-$BiVO_4$ is delivering a higher photocurrent than $BiVO_4$ and thus, the improved kinetics of water oxidation and surface passivation brought by the $NiFeO_x$ should result in a more significant amelioration of the $BiVO_4$ photocurrent. To elucidate the effect of the $NiFeO_x$, the η_{sep} and η_{tran} values were estimated. As observed in **Figure 3b**, whereas the η_{sep} barely changes in the case of $BiVO_4$, a significant improvement is detected when V-$BiVO_4$ is coated with $NiFeO_x$. This could be accounted for by the different band alignment at the (V -$BiVO_4$/$NiFeO_x$) interface, owing to the upwards shift of the V-$BiVO_4$ energy band with respect to those of $BiVO_4$. Indeed, Hilbrands et al. reported that the change in the $BiVO_4$ band positions caused by the different surface terminations significantly affects the charge separation.[17] Therefore, we propose that the equilibration between the V-$BiVO_4$ and the $NiFeO_x$ could trigger to strengthening of the built-in electric field, hence causing a drastic change of the η_{sep}; whereas in the $BiVO_4$/$NiFeO_x$ heterojunction this may remain unaltered. This hypothesis is consistent with the distinct change of the V_{ph} for the $NiFeO_x$-coated $BiVO_4$ and V-$BiVO_4$. As observed in **Figure 3c**, the $NiFeO_x$ deposition caused the V_{ph} to increase about 45 mV and 80 mV for $BiVO_4$ and V-$BiVO_4$, respectively (Figure S7). The former could be accounted for by the hole transfer to the $NiFeO_x$, whereas the larger band bending could explain the additional increase of the V_{ph} observed in the latter. Close examination of the η_{tran} reveals that the $NiFeO_x$ affects both $BiVO_4$ and V-$BiVO_4$ in the same extent, reaching values ca. 60% and 80%, respectively. While the improved η_{tran} primarily stemmed from the amelioration of the OER kinetics, the distinct values might be dictated by the surface recombination. Indeed, FS-CVs revealed that the overlayer of $NiFeO_x$ further contributed to reduce the Q_{r-SS}, likely because of its ability to accept photogenerated holes, and that $NiFeO_x$-coated V-$BiVO_4$ displays the lowest Q_{r-SS}, thus, potentially the lowest degree of surface recombination (**Figure 3f**). Finally, the stability of the $NiFeO_x$-modified electrodes was tested (Figure S11). Interestingly, while the $NiFeO_x$-coated $BiVO_4$ displayed about a 44% photocurrent loss after 10 h of operation, the counterpart based on V-$BiVO_4$ retained about 93% of the photocurrent. These results agree well with those reported by Tran-Phu et al.[19] wherein they noticed a faster leaching of vanadium, and therefore a shorter lifespan under operative conditions, for V-poor $BiVO_4$. Note that we often detect an initial improvement in the photocurrent in some samples in the first hour, as it is exemplified in the case of V-$BiVO_4$, which we attributed to the preconditioning or activation of part of the catalyst.

Scheme 2 shows the tentative energy diagrams for $BiVO_4$ and V-$BiVO_4$ and the corresponding illustrations that portray the change in the surface termination, as concluded from the results. As observed, the filling of the native V vacancies upon the NH_4VO_3 treatment caused the E_{FB} to shift upwards (in the energy scale) while reducing the density of r-SS, which are identified as the main surface recombination centers. Likewise, the increased density of oxygen vacancies caused an increased carrier density (see supporting info semiquantitative energy bands calculation). As a result, under the same applied potential, V-$BiVO_4$ displays a larger built-in electric field favoring, thus, the charge separation in the bulk. Likewise, the passivation of the r-SS mitigates the deleterious surface recombination that competes with the OER. Coating with $NiFeO_x$ primarily mitigates the surface recombination, as depicted by the drop in Q_{r-SS}, while improving the kinetics of water oxidation. However, we hypothesize that the distinct equilibration between the V-$BiVO_4$ and $NiFeO_x$ caused to further shift upwards the V-$BiVO_4$ energy bands with respect to those of $BiVO_4$ reinforcing the band bending and, hence, the charge separation.

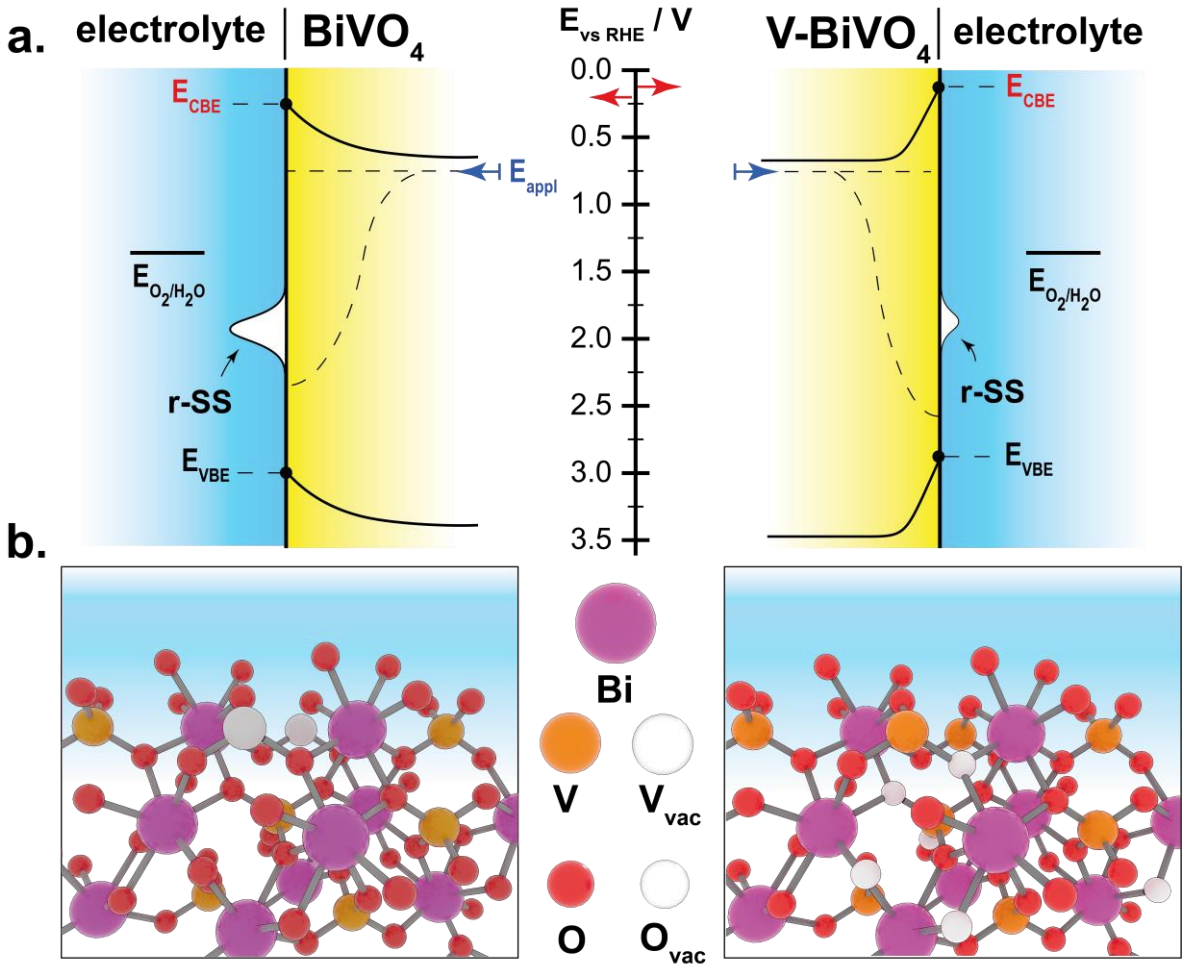

Scheme 2. (a) Tentative energy diagrams for $BiVO_4$ and V-$BiVO_4$ portraying the differences in the energy of conduction band edge (E_{CBE}, indicated with red arrow) and of the valence band edge (E_{VBE}), the built-in electric field and the density of r-SS. **(b)** Illustration of the atomic structure indicating the native occurrence of vanadium vacancies in pristine $BiVO_4$, and the subsequent filling of such traps together with the formation of oxygen vacancies, preferentially Bi-O-Bi bridges, in V-$BiVO_4$.

Conclusions

In this study, we tackle the commonplace limitations on bulk transport and the severe recombination of $BiVO_4$ photoanodes by tailoring the surface termination and parsing out the effects on the PEC response. By annealing in the presence of NH_4VO_3, we found that the native surface Bi:V ratio of 2.3 could be precisely modulated down to 1.3, while the density of oxygen vacancies increased, without noticeable changes on the morphology or the crystal structure. PEC tests revealed that the optimized NH_4VO_3-treated sample (V-$BiVO_4$) displayed improved V_{on} and photocurrent with respect to pristine $BiVO_4$. On the one hand, the generation of oxygen vacancies in the bulk was found to be behind the relatively modest improvement of charge separation by increasing the band bending, as confirmed by the OCP measurements and EIS. Indeed, the latter evidenced an upward shift of the V-$BiVO_4$ energy bands with respect to $BiVO_4$ that further contributed to achieving a larger band bending and V_{on}. On the other hand, FS-CVs measurements provided compelling evidence that the amelioration of the charge transfer across the liquid interface was primarily caused by the passivation of the recombination centers. These, based on XPS data, were attributed to V vacancies that could be filled by means of the NH_4VO_3 treatment. Overall, the fact that the change of η_{tran} was larger than that of η_{sep} emphasized that the surface passivation was the main phenomenon controlling the improved performance of V-$BiVO_4$. Subsequent incorporation of $NiFeO_x$ led to an enhanced PEC response particularly pronounced in the case of the V-$BiVO_4$. The detailed characterization of the samples revealed a superior enhanced of the charge separation in the case of V-$BiVO_4$, probably derived from a more suitable equilibration with $NiFeO_x$, and this, ultimately, led to the improvement of the PEC performance. In a more general vein, our

findings established a new strategy to precisely tune the surface termination and affect the surface recombination and energetics, which we believe will guide further optimization of $BiVO_4$ and other emerging metal oxides, and inspire new treatments to control the surface stoichiometry.

Supporting Information

Experimental details, Figures S1−S11 and Table S1-S4 as described in the main text, and additional information regarding the interpretation of some of the results presented herein are available.

Acknowledgements

J.L. acknowledges the funding support from the National Key Research and Development Program of China (Grant No. 2019YFE0123400), the Excellent Young Scholar Fund from the National Science Foundation of China (22122903), the Tianjin Distinguished Young Scholar Fund (20JCJQJC00260) and the "111" Project (Grant No. B16027). Q.W. acknowledges the funding support from the China Scholarship Council (202206200070). N.G. thanks the Spanish Ministry of Science & Innovation for the "Ramon y Cajal" Program (RYC2018-023888-I) and for support via de project TED2021-132697B-100. This project has also received funding from the European Research Council (ERC) under the European Union's Horizon 2020 research and innovation programme (grant agreement No.948829).

Reference

1. Kang, D.; Kim, T. W.; Kubota, S. R.; Cardiel, A. C.; Cha, H. G.; Choi, K.-S., Electrochemical Synthesis of Photoelectrodes and Catalysts for Use in Solar Water Splitting. *Chem. Rev* **2015,** *115*, 12839-12887.
2. Wang, S.; Liu, G.; Wang, L., Crystal Facet Engineering of Photoelectrodes for Photoelectrochemical Water Splitting. *Chem. Rev* **2019,** *119*, 5192−5247.
3. Park, Y.; McDonald, K. J.; Choi, K.-S., Progress in bismuth vanadate photoanodes for use in solar water oxidation. *Chem. Soc. Rev* **2013,** *42* (6), 2321-2337.
4. Kim, J. H.; Lee, J. S., Elaborately Modified $BiVO_4$ Photoanodes for Solar Water Splitting. *Adv. Mater* **2019,** *31*, 1806938.
5. Zhang, X.; Zhai, P.; Zhang, Y.; Wu, Y.; Wang, C.; Ran, L.; Gao, J.; Li, Z.; Zhang, B.; Fan, Z.; Sun, L.; Hou, J., Engineering Single-Atomic Ni-N_4-O Sites on Semiconductor Photoanodes for High-Performance Photoelectrochemical Water Splitting. *Journal of the American Chemical Society* **2021,** *143* (49), 20657-20669.
6. Zhang, Z.; Huang, X.; Zhang, B.; Bi, Y., High-performance and stable $BiVO_4$ photoanodes for solar water splitting via phosphorus-oxygen bonded FeNi catalysts. *Energy & Environmental Science* **2022,** *15* (7), 2867-2873.
7. Xiaoxia Chang; Tuo Wang; Peng Zhang; Jijie Zhang; Ang Li; Gong, J., Enhanced Surface Reaction Kinetics and Charge Separation of p−n Heterojunction Co_3O_4/$BiVO_4$ Photoanodes. *Journal of the American Chemical Society* **2015,** *137* (26), 8356-8359.
8. Zhang, R.; Ning, X.; Wang, Z.; Zhao, H.; He, Y.; Han, Z.; Du, P.; Lu, X., Significantly Promoting the Photogenerated Charge Separation by Introducing an Oxygen Vacancy Regulation Strategy on the FeNiOOH Co-Catalyst. *Small* **2022,** *18* (20), 2107938.
9. Tang, R.; Zhou, S.; Zhang, Z.; Zheng, R.; Huang, J., Engineering Nanostructure–Interface of Photoanode Materials Toward Photoelectrochemical Water Oxidation. *Adv. Mater* **2021**, 2005389.
10. Liu, B.; Wang, X.; Zhang, Y.; Xu, L.; Wang, T.; Xiao, X.; Wang, S.; Wang, L.; Huang, W., A $BiVO_4$ Photoanode with a VO_x Layer Bearing Oxygen Vacancies Offers Improved Charge Transfer and Oxygen Evolution Kinetics in Photoelectrochemical Water Splitting. *Angewandte Chemie International Edition* **2023,** *62* (10), e202217346.
11. Jian, J.; Xu, Y.; Yang, X.; Liu, W.; Fu, M.; Yu, H.; Xu, F.; Feng, F.; Jia, L.; Friedrich, D.; Krol, R. v. d.; Wang, H., Embedding laser generated nanocrystals in $BiVO_4$ photoanode for efficient photoelectrochemical water splitting. *Nature Communications* **2019,** *10* (1), 2609-2618.
12. Zhang, B.; Yu, S.; Dai, Y.; Huang, X.; Chou, L.; Lu, G.; Dong, G.; Bi, Y., Nitrogen-incorporation activates $NiFeO_x$ catalysts for efficiently boosting oxygen evolution activity and stability of $BiVO_4$ photoanodes. *Nature Communications* **2021,** *12* (1), 6969-677.
13. Jung Kyu Kim; Xinjian Shi; Myung Jin Jeong; Joonsuk Park; Hyun Soo Han; Suk Hyun Kim; Yu Guo, T. F. H., Shanhui Fan, Chang-Lyoul Lee, Jong Hyeok Park; Zheng, X., Enhancing Mo:$BiVO_4$ Solar Water Splitting with Patterned Au Nanospheres by Plasmon-Induced Energy Transfer. *Advanced Energy Materials* **2018,**

8 (5), 1701765.
14. Li, L.; Yang, X.; Lei, Y.; Yu, H.; Yang, Z.; Zheng, Z.; Wang, D., Ultrathin Fe-NiO nanosheets as catalytic charge reservoirs for a planar Mo-doped $BiVO_4$ photoanode. *Chemical Science* **2018,** *9* (47), 8860-8870.
15. Abdi, F. F.; Han, L.; Smets, A. H. M.; Zeman, M.; Dam, B.; Krol, R. v. d., Efficient solar water splitting by enhanced charge separation in a bismuth vanadate-silicon tandem photoelectrode. *Nature communications* **2013,** *4* (1), 2195-2202.
16. Lee, D.; Wang, W.; Zhou, C.; Tong, X.; Liu, M.; Galli, G.; Choi, K.-S., The impact of surface composition on the interfacial energetics and photoelectrochemical properties of $BiVO_4$. *Nature Energy* **2021,** *6* (3), 287-297.
17. Hilbrands, A. M.; Zhang, S.; Zhou, C.; Melani, G.; Wi, D. H.; Lee, D.; Xi, Z.; Head, A. R.; Liu, M.; Galli, G.; Choi, K. S., Impact of Varying the Photoanode/Catalyst Interfacial Composition on Solar Water Oxidation: The Case of $BiVO_4$(010)/FeOOH Photoanodes. *J Am Chem Soc* **2023,** *145* (43), 23639-23650.
18. Lu, Y.; Yang, Y.; Fan, X.; Li, Y.; Zhou, D.; Cai, B.; Wang, L.; Fan, K.; Zhang, K., Boosting Charge Transport in $BiVO_4$ Photoanode for Solar Water Oxidation. *Advanced Materials* **2022,** *34* (8), 2108178.
19. Tran-Phu, T.; Fusco, Z.; Di Bernardo, I.; Lipton-Duffin, J.; Toe, C. Y.; Daiyan, R.; Gengenbach, T.; Lin, C.-H.; Bo, R.; Nguyen, H. T.; Barca, G. M. J.; Wu, T.; Chen, H.; Amal, R.; Tricoli, A., Understanding the Role of Vanadium Vacancies in $BiVO_4$ for Efficient Photoelectrochemical Water Oxidation. *Chemistry of Materials* **2021,** *33* (10), 3553-3565.
20. Venugopal, A.; Kas, R.; Hau, K.; Smith, W. A., Operando Infrared Spectroscopy Reveals the Dynamic Nature of Semiconductor-Electrolyte Interface in Multinary Metal Oxide Photoelectrodes. *J Am Chem Soc* **2021,** *143* (44), 18581-18591.
21. Kim, T. W.; Choi, K.-S., Nanoporous $BiVO_4$ Photoanodes with Dual-Layer Oxygen Evolution Catalysts for Solar Water Splitting. *Science* **2014,** *343* (6174), 990-994.
22. Zou, J.; Cai, Z.; Lai, Y.; Tan, J.; Zhang, R.; Feng, S.; Wang, G.; Lin, J.; Liu, B.; Cheng, H. M., Doping Concentration Modulation in Vanadium-Doped Monolayer Molybdenum Disulfide for Synaptic Transistors. *ACS Nano* **2021,** *15* (4), 7340-7347.
23. Tolod, K. R.; Saboo, T.; Hernández, S.; Guzmán, H.; Castellino, M.; Irani, R.; Bogdanoff, P.; Abdi, F. F.; Quadrelli, E. A.; Russo, N., Insights on the surface chemistry of $BiVO_4$ photoelectrodes and the role of Al overlayers on its water oxidation activity. *Applied Catalysis A: General* **2020,** *605*.
24. Rossell, M. D.; Agrawal, P.; Borgschulte, A.; Hébert, C.; Passerone, D.; Erni, R., Direct Evidence of Surface Reduction in Monoclinic $BiVO_4$. *Chemistry of Materials* **2015,** *27* (10), 3593-3600.
25. Song, K.; Hou, H.; Gong, C.; Gao, F.; Zhang, D.; Fang Zhi; Yang, W.; He, F., Enhanced solar water splitting of $BiVO_4$ photoanodes by in situ surface band edge modulation. *Journal of Materials Chemistry A* **2022,** *10* (42), 22561-22570.
26. Kim, D. S.; Lee, K. W.; Choi, J. H.; Lee, H. H.; Suh, H. W.; Lee, H. S.; Cho, H. K., Durable VO_2 transition layer and defect inactivation in $BiVO_4$ via spontaneous valence-charge control. *Journal of Materials Chemistry A* **2022,** *10* (40), 21300-21314.
27. Qingjie Wang; Linxiao Wu; Zhuang Zhang; Jinshui Cheng; Rong Chen; Yang Liu; Luo, J., Elucidating the Role of Hypophosphite Treatment in Enhancing the Performance of $BiVO_4$ Photoanode for Photoelectrochemical Water Oxidation. *ACS Applied Materials & Interfaces* **2022,** *14* (23), 26642-26652.
28. Bi, Y.; Yang, Y.; Shi, X. L.; Feng, L.; Hou, X.; Ye, X.; Zhang, L.; Suo, G.; Chen, J.; Chen, Z. G., Bi_2O_3/$BiVO_4$@graphene oxide van der Waals heterostructures with enhanced photocatalytic activity toward oxygen generation. *J Colloid Interface Sci* **2021,** *593*, 196-203.
29. Wan, S.; Dong, C.; Jin, J.; Li, J.; Zhong, Q.; Zhang, K.; Park, J. H., Tuning the Surface Wettability of a $BiVO_4$ Photoanode for Kinetically Modulating Water Oxidative H_2O_2 Accumulation. *ACS Energy Letters* **2022,** *7*, 3024-3031.
30. Wang, S.; He, T.; Chen, P.; Du, A.; Ostrikov, K. K.; Huang, W.; Wang, L., In Situ Formation of Oxygen Vacancies Achieving Near-Complete Charge Separation in Planar $BiVO_4$ Photoanodes. *Advanced Materials* **2020,** *32* (26), 2001385.
31. Shuang-Feng Yin, J.-B. P., Bing-Hao Wang, Jin-Bo Wang, Hong-Zhi Ding, Wei Zhou, Xuan Liu, Jin-Rong Zhang, JunKang Guo, Li-Long Jiang, Sheng Shen, Lang Chen, Chak-Tong Au, Activity and Stability Boosting of Oxygen-Vacancy-Rich $BiVO_4$ Photoanode by NiFe-MOFs Thin Layer for Water Oxidation. *Angewandte Chemie International Edition* **2021,** *60* (3), 1433-1440.
32. Songcan Wang; Peng Chen; Jung-Ho Yun; Yuxiang Hu; Wang, L., An Electrochemically Treated $BiVO_4$ Photoanode for Efficient Photoelectrochemical Water Splitting. *Angewandte Chemie* **2017,** *129* (29), 8620-8624.
33. Dupin, J.-C.; Gonbeau, D.; Vinatier, P.; Levasseur, A., Systematic XPS studies of metal oxides, hydroxides and peroxides. *Physical Chemistry Chemical Physics* **2000,** *2* (6), 1319-1324.
34. Lampe-Onnerud, C.; Thomas, J., Mechanisms for the Thermal Decomposition of NH_4V0_3 into V_60_{13}, V_30_7 and V_2O_5. *Journal of Materials Chemistry* **1995,** *5* (7), 1075-1080.
35. Kim, T. W.; Ping, Y.; Galli, G. A.; Choi, K.-S., Simultaneous enhancements in photon absorption and

charge transport of bismuth vanadate photoanodes for solar water splitting. *Nature communications* **2015,** *6* (1), 8769-8779.
36. Li, G.-L., First-principles investigation of the surface properties of fergusonite-type monoclinic $BiVO_4$ photocatalyst. *RSC Advances* **2017,** *7* (15), 9130-9140.
37. Song, K.; He, F.; Zhou, E.; Wang, L.; Hou, H.; Yang, W., Boosting solar water oxidation activity of $BiVO_4$ photoanode through an efficient in-situ selective surface cation exchange strategy. *Journal of Energy Chemistry* **2022,** *68*, 49-59.
38. Cui, J.; Daboczi, M.; Regue, M.; Chin, Y. C.; Pagano, K.; Zhang, J.; Isaacs, M. A.; Kerherve, G.; Mornto, A.; West, J.; Gimenez, S.; Kim, J. S.; Eslava, S., 2D Bismuthene as a Functional Interlayer between $BiVO_4$ and NiFeOOH for Enhanced Oxygen-Evolution Photoanodes. *Advanced Functional Materials* **2022,** *32* (44), 2207136.
39. Chen, H.; Li, J.; Yang, W.; Balaghi, S. E.; Triana, C. A.; Mavrokefalos, C. K.; Patzke, G. R., The Role of Surface States on Reduced TiO_2@$BiVO_4$ Photoanodes: Enhanced Water Oxidation Performance through Improved Charge Transfer. *ACS Catal* **2021,** *11*, 7637−7646.
40. Shi, Q.; Murcia-López, S. n.; Tang, P.; Flox, C.; Morante, J. R.; Bian, Z.; Wang, H.; Andreu, T., Role of Tungsten Doping on the Surface States in $BiVO_4$ Photoanodes for Water Oxidation: Tuning the Electron Trapping Process. *ACS Catal* **2018,** *8*, 3331−3342.